

NO TENSION: JWST GALAXIES AT $z > 10$ CONSISTENT WITH COSMOLOGICAL SIMULATIONS

JOE M. MCCAFFREY^{1,*}, SAMANTHA E. HARDIN², JOHN H. WISE², AND JOHN A. REGAN¹

¹Centre for Astrophysics and Space Science Maynooth, Department of Theoretical Physics, Maynooth University, Maynooth, Ireland

²Center for Relativistic Astrophysics, Georgia Institute of Technology, 837 State Street, Atlanta, GA 30332, USA

Version September 27, 2023

ABSTRACT

Recent observations by JWST have uncovered galaxies in the very early Universe via the JADES and CEERS surveys. These galaxies have been measured to have very high stellar masses with substantial star formation rates. There are concerns that these observations are in tension with the Λ CDM model of the Universe, as the stellar masses of the galaxies are relatively high for their respective redshifts. Recent studies have compared the JWST observations with large-scale cosmological simulations. While they were successful in reproducing the galaxies seen in JADES and CEERS, the mass and spatial resolution of these simulations were insufficient to fully capture the early assembly history of the simulated galaxies. In this study, we use results from the **Renaissance** simulations, which are a suite of high resolution simulations designed to model galaxy formation in the early Universe. We find that the most massive galaxies in **Renaissance** have stellar masses and star formation rates that are consistent with the observations from the JADES and CEERS surveys. The higher resolution afforded by **Renaissance** allows us to model the build-up of early galaxies from stellar masses as low as $10^4 M_{\odot}$ up to a maximum stellar mass of a few times $10^7 M_{\odot}$. Within this galaxy formation paradigm, and after extrapolating forward in time the stellar masses in Renaissance where required, we find overall agreement with JADES and CEERS. We find no tension between the Λ CDM model and current JWST measurements. As JWST continues to explore the high redshift Universe, simulations, such as **Renaissance**, will continue to be crucial in understanding the formation history of early embryonic galaxies.

Keywords: JWST, Galaxies, Cosmological Simulations, High-Redshift.

1. INTRODUCTION

With the launch, and now the first observations with JWST, the high-redshift Universe is being unveiled with unprecedented detail for the first time. As exquisitely detailed measurements of distant early galaxies are now within range of observations, it allows for the opportunity to compare the results of these observations against high resolution simulations of early galaxy formation which was previously intractable.

The JADES survey (Bunker 2019) has provided measurements on five galaxies with spectroscopically confirmed redshifts at $z > 10$. Three of these galaxies are the most distant yet detected. Robertson et al. (2022), Curtis-Lake et al. (2022) and Bunker et al. (2023) have constrained physical properties of these five galaxies, finding that the galaxies lie at (mean) spectroscopic redshifts of $z = 10.38$ (GS-z10-0), $z = 11.58$ (GS-z11-0), $z = 12.63$ (GS-z12-0), $z = 13.20$ (GS-z13-0) and $z = 10.60$ (GN-z11). Additionally the CEERS project (Finkelstein et al. 2022a) has also provided measurements for Maisie’s galaxy which has a redshift of 11.44 (Arrabal Haro et al. 2023). In total there are six spectroscopically confirmed galaxies against which we can directly compare.

The JADES survey, performed using the NIRC*am* instrument on JWST, targets a region, previously studied by the Hubble Telescope (Beckwith et al. 2006), in nine different wavelength ranges. JADES was conducted with the aim of detecting faint galaxies using the dropout-technique (Bunker 2019) allowing for fast identification

of high redshift galaxy candidates. However, the photometry alone is not enough to confirm the candidates’ redshift and a follow-up spectrum, using an instrument like NIRS*pec*, is needed to confidently quantify the redshift of the candidates as noted above.

Similar to JADES, CEERS aims to study the first 500 Myr of galaxy evolution again by using a combination of the NIRC*am* instrument for fast identification followed by a longer duration follow-up using NIRS*pec*. Initial photometric measurements of Maisie’s galaxy and of CEERS-93316 placed them at photometric redshifts of $z_{\text{phot}} = 11.08$ (Finkelstein et al. 2022b) and $z_{\text{phot}} = 16.45$ (Donnan et al. 2022), respectively. Spectroscopic follow-up measurements of these galaxies confirmed their redshifts to be $z_{\text{spec}} = 11.44$ and $z_{\text{spec}} = 4.912$ (Arrabal Haro et al. 2023), respectively. Due to the decrease in redshift of CEERS-93316 to a much lower redshift, we do not include it in the analysis in this paper and instead only include the high redshift Maisie’s galaxy.

The spectra of the galaxies found in JADES and CEERS were analysed using **Beagle** (Chevallard & Charlot 2016), to estimate the stellar mass and star formation rate of each galaxy which we compare directly against our simulations. More details on the modelling procedure used to reduce the observational data can be found in the detection papers (e.g. Bunker et al. 2023; Arrabal Haro et al. 2023).

In a recent study (Keller et al. 2023, hereafter K23) tested the capabilities of a variety of cosmological simulations by investigating whether these simulations were able to reproduce galaxies with properties similar to the galaxies observed in the JADES and CEERS surveys.

*E-mail: joe.mccaffrey@mu.ie

To do this, K23 utilised EAGLE (McAlpine et al. 2016), Illustris (Vogelsberger et al. 2014), TNG100 (Naiman et al. 2018), RomulusC (Tremmel et al. 2018), OBELISK (Trebitsch et al. 2021) and Simba (Davé et al. 2019).

K23 concluded that the cosmological simulations they examined were able to reproduce galaxies with a similar stellar mass and star formation rate (SFR) compared to the galaxies observed in the JADES simulations and that the observed galaxies are consistent with a flat Λ CDM model. In this paper, we build-on the work of K23 by comparing the JADES and CEERS results against high resolution simulations that were designed to specifically examine a high-redshift environment and to model the early assembly history of the first galaxies. By considering simulation data from both the higher halo mass regime of K23 and the lower halo mass data from this paper, we strengthen the argument that there exists no tension between the measurements of JWST and the Λ CDM model of the Universe.

This study accomplishes this using the **Renaissance** simulation suite (Xu et al. 2013; Chen et al. 2014; O’Shea et al. 2015). The **Renaissance** simulations model early galaxy formation in three regions which differ from each other by their level of overdensity (see O’Shea et al. 2015, for details). Using a similar methodology to K23, we compare the results from these simulations to the JADES and CEERS galaxy property estimates, observationally validating our simulation results and also determining the likeliness of such massive galaxies forming early in a Λ CDM cosmology.

There have been significant concerns that the early measurements by JWST are in conflict with the Λ CDM model of the Universe. In particular, there are claims that the stellar masses of the galaxies observed by JWST are simply too high to be explained in the context of a Λ CDM cosmology (e.g. Haslbauer et al. 2022) and that the masses of the JWST galaxies, as measured at redshifts between 7 and 10 by Labbe et al. (2022) in particular, are testing the upper limits on the available baryonic mass available according to Λ CDM (Boylan-Kolchin 2023). See also Lovell et al. (2023), Dekel et al. (2023), Harikane et al. (2023), Steinhardt et al. (2023), Menci et al. (2022), and Mason et al. (2023) for more discussion and analysis on the proposed tension between the JWST measurements and Λ CDM.

This paper addresses these concerns by showing that simulations (based on a Λ CDM cosmology) are able to reproduce galaxies consistent with the early findings of JWST at least at the very highest redshifts explored by it. If the Labbe et al. (2022) result holds under spectroscopic scrutiny and the galaxies are found to lie in typical regions of a Λ CDM Universe, then, as pointed out by Boylan-Kolchin (2023), this represents a major challenge to standard cosmology. However, see also Prada et al. (2023) which offers an alternative explanation to the large stellar masses found by Labbe et al. (2022).

The paper is laid out as follows: §2 describes the high-resolution **Renaissance** simulations as well as the methodology and code used to run the suite, §3 discusses the results of the analysis performed and in §4 we discuss the implications of the results and the case for further analysis of the high redshift Universe using cosmological simulations.

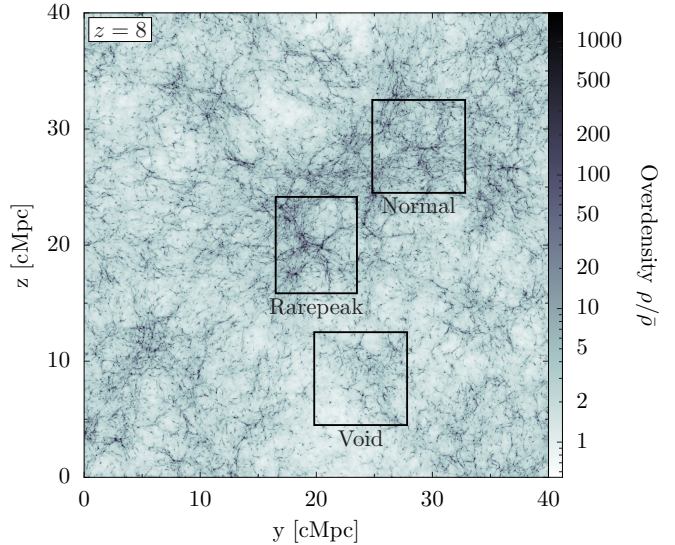


FIG. 1.— Mass-weighted density projection of the $(40 \text{ comoving Mpc})^3$ exploratory dark matter simulations at redshift $z = 8$ used in the **Renaissance** suite. The survey volumes of the Rarepeak, Normal and Void regions are outlined. The Rarepeak region is centered on the most massive halo at $z = 6$. Due to projection effects, the Normal region appears as dense as the Rarepeak region. However, the average overdensity of the Normal region is only 9% higher than the mean matter density. Visualisation originally published in Xu et al. (2016).

2. METHODOLOGY

2.1. The Renaissance Simulations

The **Renaissance** simulations (Xu et al. 2013; Chen et al. 2014; O’Shea et al. 2015; Smith et al. 2018; Wise et al. 2019) were run using the massively parallel adaptive mesh refinement **Enzo** code (Bryan et al. 2014; Brummel-Smith et al. 2019). We briefly describe the methods used here, but refer the interested reader to the previous papers for a more complete discussion. The **Renaissance** simulation suite is composed of three zoom-in regions (see Figure 1) extracted from a parent comoving volume of 40 Mpc on a side. The three separate zoom-in regions were named the Rarepeak (RP) region, the Normal region and the Void region. The zoom-in volumes ranged from 200 to 430 comoving Mpc^3 .

The RP region is centred on a $3 \times 10^{10} M_{\odot}$ halo at $z = 6$ with an enclosing comoving volume of $(3.8 \times 5.4 \times 6.6) \text{ Mpc}^3$. The Normal and Void volumes have comoving volumes of $(6.0 \times 6.0 \times 6.125) \text{ Mpc}^3$. All three regions have projected areas comparable to the NIRCcam field of view with the RP, Normal, and Void regions respectively subtending $(1.2' \times 1.8' \times 2.2')$ at $z = 15$, $(2.1' \times 2.1' \times 2.1')$ at $z = 11.6$, $(2.2' \times 2.2' \times 2.3')$ at $z = 8$. The **Renaissance** suite uses the cosmological parameters from the 7-year WMAP Λ CDM+SZ+LENS best fit (Komatsu et al. 2011) with $\Omega_{\text{M}} = 0.266$, $\Omega_{\Lambda} = 0.734$, $\Omega_{\text{b}} = 0.0449$, $h = 0.71$, $\sigma_8 = 0.81$ and $n = 0.963$. The (dark matter) particle mass resolution of the **Renaissance** suite is $2.9 \times 10^4 M_{\odot}$ and the maximum spatial resolution afforded by the adaptive mesh is 19 comoving pc. This allows the **Renaissance** suite to resolve most of the minihaloes in which the first stars are expected to form (e.g. Machacek et al. 2001; Kulkarni et al. 2021; Chiaki et al. 2023).

In particular, **Renaissance** employs a model for metal-free (Population III) and metal-poor (Population II) star formation (Wise & Cen 2009; Wise et al. 2012) allowing for the stochastic sampling of the formation of the first stars and galaxies, inspired by star formation simulations and observations rather than their galactic counterparts because they resolve individual star-forming clouds. Under the assumption that metal-enriched star formation is insensitive to redshift, Wise et al. (2012) used an efficiency of 7 per cent of the cold gas within a dense cloud being converted into Population II star particles, similar to what was found in present-day star formation simulations (Krumholz & McKee 2005), which were themselves consistent with observations (Tan et al. 2006) at the time of the method’s formulation. They calibrated the feedback models against local dwarf galaxy properties, in particular the metallicity distribution function, ensuring that they avoided the “overcooling problem” that overestimates the stellar mass and thus metallicities. The resulting metal enrichment driven from the collapse of the first stars results in the emergence of the second generation of stars which ultimately lead to the birth of the first massive galaxies - the galaxies which JWST is now observing.

The computational complexity of the **Renaissance** suite means that evolving these simulations to the present day is completely intractable. As such the RP simulation was evolved to $z = 15$, the Normal simulation evolved to $z = 11.6$ and the Void region to $z = 8$. As some of the JADES and CEERS results are at somewhat lower redshifts (compared to the RP and Normal runs) we extrapolate our results to the JADES and CEERS spectroscopic redshifts in some cases.

As discussed in the Introduction, the comparison study undertaken by K23 uses the simulation datasets from EAGLE, Illustris, TNG100, RomulusC, OBELISK and Simba. In Table 1 we compare the simulation datasets used in K23 versus that used here (i.e. against **Renaissance**). The simulations used in K23 do not have sufficient resolution to probe the formation of the first stars and can resolve, at best, the formation of the first atomic cooling haloes. The **Renaissance** suite allows us to probe the assembly processes involved in forming the haloes that appear in the simulations used in K23 as well as the building blocks of the galaxies now being observed with JWST.

2.2. Extrapolating the Stellar Mass of the Simulated Galaxies based on the Star Formation History

To properly compare the simulated galaxy conditions against observations, we need to have simulated values at the same redshift as the JADES and CEERS measurements. However, as discussed, both the Normal and RP regions of the **Renaissance** simulations only reach a redshift of $z = 11.6$ and $z = 15$ respectively. Therefore, the Normal region does not reach sufficiently low redshifts so as to be directly comparable against two of the JADES and CEERS galaxies, while the RP region cannot be directly compared, in terms of redshift, against any of the JADES and CEERS galaxies. To rectify this, we extrapolate the stellar masses of the most massive galaxy in both the Normal and RP region based on their

TABLE 1
SIMULATION DOMAIN SIZES AND RESOLUTION

Simulation	Box size [cMpc]	M_{DM} [M_{\odot}]	$\Delta x_{\text{DM},*}$ [pc]
Simba	147.7	9.7×10^7	500
EAGLE	100	9.7×10^6	2660
TNG100	110.7	7.5×10^6	740
Illustris	106.5	6.3×10^6	710
OBELISK	142.0	1.2×10^6	540
RomulusC	50	3.4×10^5	250
Renaissance	40	2.4×10^4	19

Notes: The first column gives the simulation suite name, the second column the comoving box size length of each simulation used in K23, the third column gives the dark matter particle resolution, M_{DM} , and finally the fourth column gives the spatial resolution. The spatial resolution was based on the gravitational softening lengths for the SPH simulations and for the AMR simulations it is based on the cell length. For the **Renaissance** suite we give the parent box size (40 cMpc) but note that the results we show here are for the zoom in regions which have box lengths of approximately 6 cMpc.

respective specific Star Formation Rates (sSFR) forward in time to connect with the observational redshifts.

The definition of the sSFR is

$$\Psi_{\text{S}} \equiv \frac{\Psi}{M_{*}} \quad (1)$$

where Ψ is the SFR and M_{*} is the stellar mass. We use three values for Ψ_{S} in our extrapolation method: A maximum value of 10^{-7} yr^{-1} , a nominal value of 10^{-8} yr^{-1} , and a minimum value of 10^{-9} yr^{-1} . These values were chosen from the range of sSFR values found in **Renaissance** (see also Figure 4). The extrapolated mass is dictated by the differential equation

$$\Psi \equiv \frac{dM_{*}}{dt} = \Psi_{\text{S}} M_{*}, \quad (2)$$

where the solution of this equation is

$$M_{*}(t) = M_0 e^{\Psi_{\text{S}}(t-t_0)}. \quad (3)$$

Here, M_0 is the final simulated stellar mass of the halo and t_0 is the final simulated time. Using Equation (3) we can then predict the stellar mass of the galaxy past the final simulation time. We will discuss the impact of this extrapolation method in more detail next.

3. RESULTS

We begin here by comparing the most massive galaxy in each of the RP, Normal and Void regions against the JADES and CEERS results. We then follow this by comparing the global galaxy assembly history of all of the galaxies in the **Renaissance** suite against the JADES and CEERS results.

3.1. Comparing the Most Massive Galaxies in Renaissance with the JADES and CEERS measurements

In Figure 2 we plot the stellar masses of the most massive galaxy in each region in **Renaissance** against the stellar masses of each of the JADES and CEERS survey galaxies. As discussed in §2.2, we extrapolate the stellar masses to the observed redshifts for the comparison.

From Figure 2 we can immediately see that the most massive galaxy in the Normal region (blue line), which evolves to a $z = 11.6$, has a stellar mass greater than GS-z10-0 and is consistent with or within a factor of a few

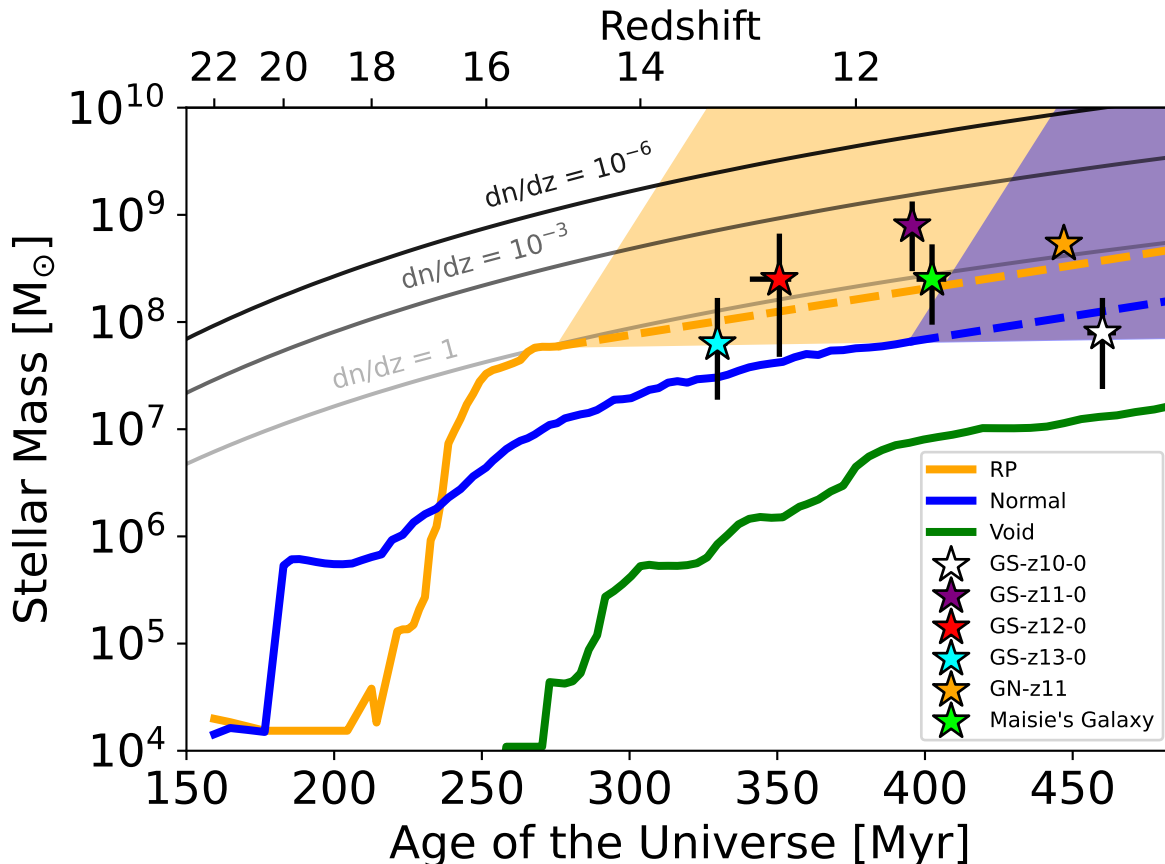


FIG. 2.— The most massive galaxy in each of the Rarepeak (RP, orange), Normal (blue) and Void (green) regions are shown. The six star shaped symbols identify the JADES and CEERS galaxies giving both their stellar masses and the redshift at which they were spectroscopically identified. The most massive galaxies in both the RP and the Normal regions are in excellent agreement with the JADES and CEERS observations. The shaded region denotes the extrapolation of the stellar masses based on the SFR history of the respective galaxy where the region is bounded from above by a specific star formation rate of 10^{-7} yr^{-1} and from below by a sSFR of 10^{-9} yr^{-1} . The dashed line represents an extrapolated mass based on a sSFR of 10^{-8} yr^{-1} . Finally, we plot lines labelled by dn/dz the expectation value for finding a galaxy of a given stellar mass at a given redshift in a field of view comparable to NIRCam. For this we assume a gas mass corresponding to the baryon fraction and a star formation efficiency (SFE) of 0.1 using the Sheth-Tormen (Sheth & Tormen 1999) halo mass function as the underlying framework. All of the JADES, CEERS and Renaissance haloes are consistent with Λ CDM predictions of finding at least one halo with these stellar masses in this volume. See text for further details on the consistency with respect to Λ CDM predictions.

compared to the stellar mass of the remaining five galaxies. The RP region, which does not overlap in redshift with any of the JADES and CEERS galaxies, is consistent in terms of stellar mass with each of the observed galaxies once extrapolation (using the sSFR) is considered. The upper bounds of both shaded regions is based on a constant sSFR value of 10^{-7} yr^{-1} , the lower bounds being 10^{-9} yr^{-1} , and the dashed lines show the extrapolated stellar masses based on a nominal sSFR value of 10^{-8} yr^{-1} . The dashed line belonging to the RP region is overall consistent with each of the observed galaxies, with GS-z11-0 and GN-z11 lying within the bounds of the extrapolations. The Void region shows systematically lower stellar masses and does not achieve the same stellar masses as those found in JADES and CEERS.

Large-scale overdensities are directly related to the overabundances of galaxies through the halo mass function and the halo mass – stellar mass relation, shown by Xu et al. (2016) for the Renaissance suite in particular. The observed stellar mass estimates suggest that the CEERS and JADES fields are not likely underdense

regions. However, additional work would be needed to statistically conclude that the JADES and CEERS were observed in overdense regions.

To provide additional context and to quantify the rarity of haloes at these masses and redshifts, we plot lines in Figure 2 to represent the number of haloes of a certain (stellar) mass we expect JWST to see at a specific redshift. These lines are based on the baryon fraction obtained from WMAP7 and a star formation efficiency (SFE) of $f_* \equiv M_* / [(\Omega_b / \Omega_M) M_{\text{halo}}] = 0.1$, with the baryonic fraction being $\Omega_b / \Omega_M \sim 0.17$. While this value for the SFE may seem high (see e.g. Tacchella et al. 2018) for this redshift regime, Renaissance shows an increasing SFE value dependent on the halo mass (see Figure 5), for this reason a value of 0.1 seems appropriate for the extrapolation. The value of $dn(M_*, z)/dz$ represents the number of galaxies of stellar mass M_* or greater we expect to see at redshift z in the NIRCcam field of view. For example $dn/dz = 10^{-3}$ tells us that we expect to see one galaxy with stellar mass M_* or greater at redshift z in every one thousand frames with the angular size of

NIRCam.

All of the galaxies are consistent with the $dn/dz = 1$ line except the GS-z11-0 galaxy whose error bars are marginally above the $dn/dz = 1$ line. This means that we should expect to observe at least one galaxy of that stellar mass in the field of view of NIRCam. The lines at $dn/dz = 10^{-3}$ and 10^{-6} represent a mass scale that would be increasingly unlikely to observe at that redshift. The calculations used in the creation of these values is described in Appendix A.

We can observe that the Normal region does not contain a galaxy that exceeds the $dn/dz = 1$ line. This can, however, be explained through cosmic variance (Chen et al. 2023; Bhowmick et al. 2020) which would provide an uncertainty in the expectation values of the stellar mass of $\sim \pm 100\%$ (e.g. Ucci et al. 2021). It may also be explained by a variance in the halo mass function used at high redshifts (Yung et al. 2023), which would provide an additional uncertainty up to an order of magnitude in the abundances of halos at fixed stellar mass. Combining these two uncertainties can easily move the $dn/dz = 1$ lines up (or down) by a factor of a few.

In summary, the JWST observed galaxies are overall consistent with both the Normal and RP regions once the extrapolation methods and cosmic variance are taken into account. Both GN-z11 and GS-z11-0 are unusual galaxies and detailed hydrodynamic simulations are clearly struggling to match their luminosities and stellar masses perfectly. It may be that these galaxies contain star formation processes not currently correctly modelled by our subgrid recipes - by this we mean that these JWST galaxies may contain stars born from an extremely top heavy IMF including a population of extremely massive stars (e.g. Charbonnel et al. 2023a; Nagele & Umeda 2023) or unusually strong bursts of star formation (e.g. Kobayashi & Ferrara 2023). In addition to this, GN-z11 shows signatures of AGN activity (Maiolino et al. 2023a; Scholtz et al. 2023) which is not currently modelled by *Renaissance* for example and the processes responsible for seeding this massive black hole may well be a factor in explaining its large luminosity. Finally, we make no attempt here to analyse absolute cosmic abundances of high mass galaxies. The galaxies found thus far by JWST at these redshifts are at the absolute limit of the *Renaissance* simulations and we are not in a position to quantify such abundances. This is due to the small volume of the *Renaissance* simulations and thus the limitation in quantifying the statistics of high mass haloes in this epoch of the Universe.

Figure 3 shows the SFR history of the most massive galaxy in the RP, Normal and Void regions - the same as Figure 2. Here and thereafter we consider the average SFR over the previous 20 Myr, i.e. the stellar mass of star particles younger than 20 Myr divided by 20 Myr. Comparing the observed (coloured symbols) and simulated galaxies (solid coloured lines), it is clear that *Renaissance* is able to reproduce galaxies with star formation rates generally consistent with the galaxies observed in JADES and CEERS. This is achieved due to the excellent mass and spatial resolution afforded by *Renaissance* which gives *Renaissance* the unique capability to follow the formation of the galaxy stellar population(s) from approximately $10^4 M_{\odot}$ up to the final

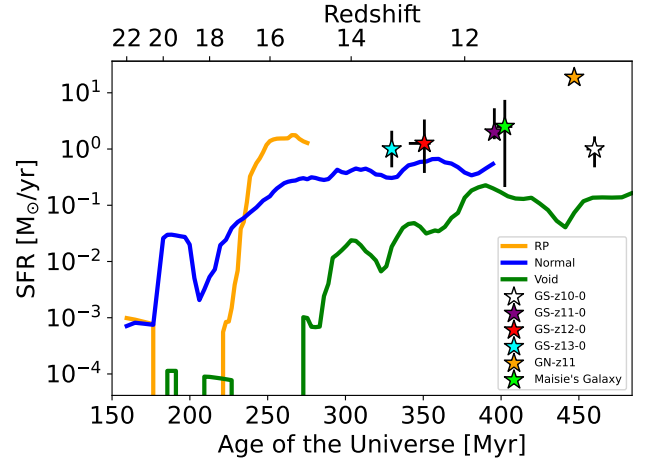


FIG. 3.— The star formation rates (SFRs) of the most massive galaxy in each of the RP (orange), Normal (blue) and Void (green) regions. The SFR of the JADES and CEERS galaxies are also plotted as star symbols with associated error bars (Robertson et al. 2022; Arrabal Haro et al. 2023; Bunker et al. 2023). All of the modelled galaxies show an initial burst of star formation at the early stages of evolution with a leveling off as each halo continues to evolve. In the cases where the observed galaxies overlap with the modelled galaxies, the SFRs found are consistent with each other within an order of magnitude. Both the Normal and RP regions show SFRs, for their highest mass galaxies of between 0.5 and $1 M_{\odot} \text{ yr}^{-1}$. The most massive galaxy in the Void region shows a lower SFR as expected (e.g. Xu et al. 2016).

simulated stellar masses of a few times $10^7 M_{\odot}$. What we see is that the star formation rates start several orders of magnitude below that observed but in very inefficient, star forming, haloes. As the star formation efficiency increases (see also Figure 4) the simulated values quickly level off to the observed values ultimately reaching values of approximately $1 M_{\odot} \text{ yr}^{-1}$.

It is the higher mass resolution of *Renaissance*, afforded through the use of adaptive grids in a zoom-in setup, that allows us to follow the build up of the galaxy from initially very small stellar masses ($\sim 10^4 M_{\odot}$) up to a final stellar mass of more than $> 10^7 M_{\odot}$. Additionally, the spatial resolution of 19 comoving pc allows for the internal structure and dynamics of these early galaxies to be well resolved.

We observe an initial burst of star formation in the *Renaissance* galaxies plotted in Figure 3 with a leveling off in the SFR as the halo continues to evolve. This can be explained via the following mechanisms. In the initial stages of star formation in the haloes, the mass resolution of *Renaissance* is sufficient to capture the early assembly history. Once the halo mass exceeds the atomic cooling threshold and gas can cool via atomic line emission, the gas begins to collapse and form Population II stars more readily and the star formation efficiency increases rapidly. The feedback from the Population II star formation heats up the surrounding environment thus regulating further star formation. This results in an equilibrium in the SFR of the halo and is represented by the leveling off seen in Figure 3.

3.2. Comparing all Galaxies in Renaissance with JADES Measurements and Simulation Results

We now expand our analysis to a larger set of high-redshift simulated galaxies to determine how the ob-

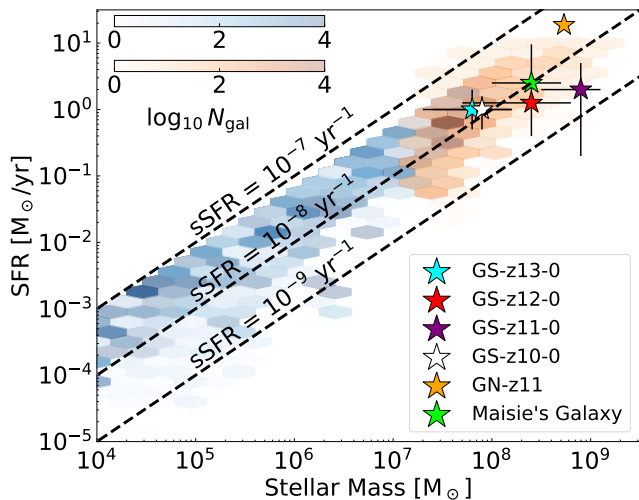


FIG. 4.— The star formation rates of the galaxies in the Renaissance simulations, which occupy lower masses in the plot and shown in blue hexbins, and the galaxies in the K23 simulations, which exist at higher masses and shown in orange hexbins, as a function of stellar mass. The bin saturation depicts the number of galaxies in a log-scale. The galaxies from the Renaissance simulations (blue hexbins) exist at redshifts greater than 15, 11.6, and 8 for the RP, Normal, and Void region, respectively. The K23 simulations are in the range of $z = 10 - 14$ for four full-box and two zoom-in simulations. We consider all outputs from the simulations as a stack over all snapshots. Lines of constant sSFR are plotted that are representative of the majority of the galaxies in the simulations. We plot the JADES and CEERS observations as stars, consistent with the simulation data.

served galaxies compare. Figure 4 shows the SFR of each galaxy as a function of the stellar mass of each galaxy in Renaissance along with the galaxies from the simulations included in K23. By including the data from our simulations and the K23 simulations, we see how both lower and higher mass galaxies compare to the JADES and CEERS data that is plotted on Figure 4 as coloured stars. The data on GS-z13-0, GS-z12-0, GS-z11-0 and GS-z10-0 are taken from Robertson et al. (2022), GN-z11 is taken from Bunker et al. (2023) while the data on Maisie’s Galaxy is taken from Arrabal Haro et al. (2023). In this comparison, we consider all galaxies in the RP, Normal, and Void regions of the Renaissance simulations that extend to very low stellar masses, shown starting from $10^4 M_{\odot}$ (blue hexbins), while the K23 simulations (orange hexbins) provide insight into the higher mass regime. As shown by Figure 4, the trends found in the Renaissance simulations compliment the K23 simulations at higher masses that overlap the JADES and CEERS observations, showing the cohesion between the simulations and observed data.

We show lines of constant sSFRs that are representative of the majority of the data in Figure 4. The figure shows that most galaxies at high-redshift quickly assemble, lying in the range $10^{-7} - 10^{-9} \text{ yr}^{-1}$ corresponding to e -folding times of 10 Myr to 1 Gyr. While it is difficult to see any definite trends in the heatmap because of the differing simulations and zoom-in regions, this figure demonstrates that early galaxy formation progresses at a fairly rapid rate with the lower mass galaxies having higher sSFR values. The plot shows that the Renaissance simulation follows closely

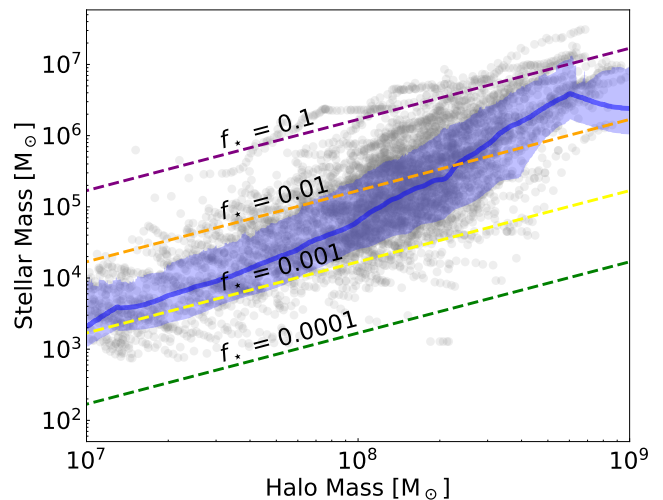


FIG. 5.— The stellar mass of each galaxy from the Renaissance simulation plotted against the halo mass of each galaxy over time. The green, yellow, orange, and purple dashed lines show the stellar mass given a constant SFE of 0.01, 0.1, 1, and 10 per cent, respectively. The blue solid line shows the median stellar mass while the shaded blue region shows the standard deviation, each of them as a function of the halo mass.

with the trend shown in the K23 simulations. For both sets of data, we can see that the distribution of the SFRs increases as stellar mass increases with a constant slope. The Renaissance data connects smoothly to the K23 and JADES data, showing how the galaxies in the Renaissance simulations could evolve over 200 Myr to become the JADES and CEERS galaxies. The consistent progression of SFR in Figure 4 from the low-mass regime (blue hexbins) to higher masses (orange hexbins) indicates that these $z > 10$ galaxies detected by JADES and CEERS are the most massive examples within a much larger and still undetected population of young and low-mass galaxies.

3.3. Simulated Stellar Mass – Halo Mass Relation

The growth of low-mass galaxies is ultimately controlled by the host dark matter halo growth, thus we turn our attention to the stellar mass - halo mass relationship of the galaxies in the Renaissance Simulations to shed light on the origins of the galaxies observed in CEERS and JADES. Figure 5 shows the stellar mass of each galaxy in the Renaissance simulation against its host halo mass from all zoom-in regions which shows the linear relationship between the halo mass and the stellar mass in the Renaissance galaxies until reaching the atomic cooling limit. We plot data from all outputs in the simulation suite. We can combine these datasets because galaxy scaling relations do not vary greatly, though with a large galaxy-to-galaxy scatter, with redshift at these early times (see Figure 15 and Table 2 in Xu et al. 2016). Here we focus on the trends between stellar mass and halo mass in this low-mass regime. From the raw data alone, there is a large scatter at all halo masses, culminating from highly variable SFRs that arise from periodic gas expulsions from stellar feedback.

To better show any trends, we show the median value (solid blue line) as a function of the halo mass for all

galaxies. We depict the standard deviation as the shaded blue region, which remains fairly constant in log-space throughout this mass range. We also show lines of constant star formation efficiency (SFE) for convenience. As demonstrated in Figure 3, galaxy growth does not proceed at a constant SFR and thus SFE, especially at these low masses when star formation can be bursty. Each galaxy makes its unique path through this parameter space. When a population of bursty galaxies are considered, these variable tracks transform into a relationship shown in the figure. Throughout most of the plot, the slope of the median line is steeper than the slopes of the constant SFE lines, meaning that the galaxies are, on average, forming stars more efficiently as they grow.

This trend clearly shows an increase in the $M_* - M_{\text{halo}}$ slope around the atomic cooling limit at $\sim 10^8 M_{\odot}$. Gas cooling and thus star formation within these nascent galaxies are inefficient below this limit with a median SFE $f_* \sim 2 \times 10^{-3}$. Once the gas can cool through atomic processes, star formation becomes more efficient, depicted by the increase in the slope and associated SFE. By the time haloes reach $10^9 M_{\odot}$, the median SFEs are a few per cent, similar to the more massive galaxies probed by the simulations highlighted in K23. With this information, we are able to justify our use for the SFE value of SFE = 0.1 that we use for the mass extrapolation discussed in §2.2.

We note that the turnover to a negative slope is an artefact of limited galaxy sample at these highest halo masses in the *Renaissance* simulations. In principle, the stellar mass should continue to grow as the halo grows. These most massive haloes have lower stellar masses than some of slightly less massive haloes. This is not unexpected because of the large scatter in the stellar mass - halo mass relation, caused by the stochastic nature of early galaxy formation.

4. DISCUSSION AND CONCLUSIONS

The goal of this study is to investigate whether or not the initial findings of JWST, via the JADES and CEERS surveys, are consistent with state-of-the-art high resolution simulations. Additionally, the high (mass) resolution simulations allow us to study in detail the assembly history of these galaxies and allow us to connect the modelled galaxies with those observed in JADES and CEERS. We find that, using the high spatial and mass resolution *Renaissance* simulations, that excellent agreement exists between observations and simulations. There is a limitation in the fact that we are unable to compare the simulations and measurements at similar redshifts. To address this, an extrapolation method was applied to the end masses of the most massive haloes in the RP and Normal regions. We justify this caveat, by extracting directly the range of sSFR values found across all halo mass ranges in *Renaissance* (see Figure 4). These sSFR values were then used to put lower and upper bounds on the mass of the most massive haloes in both the Normal and RP regions.

We also address the fact that both the GN-z11 and GS-z11-0 galaxies are above the (extrapolated) mass of the most massive galaxy in the RP region (when a sSFR of 10^{-8} yr^{-1} is used). GN-z11 was recently found to have an anomalously high abundance of N/O (Charbonnel et al. 2023b) and likely hosts an active AGN (Maiolino et al.

2023b; Scholtz et al. 2023), a characteristic that will be missed by *Renaissance*. These outliers may also be explained by an uncertainty associated with cosmic variance, as discussed in §3.1 or an uncertainty associated with the higher ends of the redshift ranges (Yung et al. 2023).

Our results are consistent with a similar study by Keller et al. (2023) who compared a range of somewhat larger scale simulations against the initial JADES and CEERS results. The combination of the larger scale study by K23 with the higher resolution simulations here, which can accurately track the initial assembly history of the galaxies subsequently found in the K23 simulations, provides compelling evidence for excellent agreement between the JADES and CEERS results and the Λ CDM model. It is the combination of the two regimes that is crucial in this regard. Our overall findings can be broken down as:

- The most massive haloes in *Renaissance* have comparable stellar masses to the JADES and CEERS galaxies after extrapolating the masses. The *Renaissance* simulation suite does not evolve in time to the same epoch as all of the observations and so we must extrapolate the (specific) star formation rate forward in time for some galaxies - but nonetheless the agreement is overall remarkable. Comparing with the theoretical expectation of galaxies within a field of view identical to NIR-Cam, we find that the $z > 10$ galaxies detected in JADES and CEERS are consistent with that expected from a Λ CDM cosmology.
- The star formation rates for the most massive galaxies in *Renaissance* are overall consistent with the JADES and CEERS measurements. The star formation histories show specific star formation rates, as a function of stellar mass, generally consistent with these latest $z > 10$ JWST observations. Finally, it is also possible that the observed stellar masses may be affected by bursts of star formation close to the epoch of observation which may effect the derived results (Narayanan et al. 2023).
- The mass resolution of *Renaissance* allows us to capture the rapid assembly of galaxies in the early Universe. After inefficiently forming stars below the atomic cooling threshold at a median SFE of 2×10^{-3} , star formation becomes more rigorous yet feedback-regulated, reaching levels of a few per cent at galaxy masses similar to the JADES and CEERS measurements.
- We conclude that both lower and finer resolution simulations agree that the JADES and CEERS measurements and are not in tension with current galaxy formation models.

JWST has for the first time enabled a detailed view of the early Universe. Initial findings of massive early galaxies has surprised many with some discussion in the literature that the JWST results maybe in conflict with Λ CDM (Haslbauer et al. 2022; Boylan-Kolchin 2023). However, what we find is that in the context of a Λ CDM Universe there is no tension between theory and observation at the very highest redshifts that we can currently probe.

As more measurements are made with JWST and future record breaking observatories, it comes with more opportunity to utilise high-resolution simulations like *Renaissance* and further stress test the Λ CDM model.

ACKNOWLEDGEMENTS

We thank the referees for providing constructive feedback and also Peter Coles for useful discussions during the course of this work. We also thank Ben Keller for providing the data points used in Figure

4. JM acknowledges the support from the John & Pat Hume Doctoral Awards Scholarship (Hume 2021-22). JR acknowledges support from the Royal Society and Science Foundation Ireland under grant number URF\R1\191132. JR also acknowledges support from the Irish Research Council Laureate programme under grant number IRCLA/2022/1165. JHW acknowledges support by NSF grants OAC-1835213 and AST-2108020 and NASA grants 80NSSC20K0520 and 80NSSC21K1053.

REFERENCES

- Arrabal Haro P., et al., 2023, Spectroscopic verification of very luminous galaxy candidates in the early universe ([arXiv:2303.15431](https://arxiv.org/abs/2303.15431))
- Beckwith S. V. W., et al., 2006, *AJ*, **132**, 1729
- Bhowmick A. K., Somerville R. S., Matteo T. D., Wilkins S., Feng Y., Tenneti A., 2020, *Monthly Notices of the Royal Astronomical Society*, 496, 754
- Boylan-Kolchin M., 2023, *Nature Astronomy*,
- Brummel-Smith C., et al., 2019, *The Journal of Open Source Software*, **4**, 1636
- Bryan G. L., Norman M. L., O’Shea B. W., Abel T., Wise J. H., Turk M. J., The Enzo Collaboration 2014, *ApJS*, **211**, 19
- Bunker A. J., 2019, *Proceedings of the International Astronomical Union*, **15**, 342
- Bunker A. J., et al., 2023, JADES NIRSpec Spectroscopy of GN-z11: Lyman- α emission and possible enhanced nitrogen abundance in a $z = 10.60$ luminous galaxy ([arXiv:2302.07256](https://arxiv.org/abs/2302.07256))
- Charbonnel C., Schaerer D., Prantzos N., Ramírez-Galeano L., Fragos T., Kuruvanthodi A., Marques-Chaves R., Gieles M., 2023a, *A&A*, **673**, L7
- Charbonnel C., Schaerer D., Prantzos N., Ramírez-Galeano L., Fragos T., Kuruvanthodi A., Marques-Chaves R., Gieles M., 2023b, *Astronomy & Astrophysics*, **673**, L7
- Chen P., Wise J. H., Norman M. L., Xu H., O’Shea B. W., 2014, *ApJ*, **795**, 144
- Chen Y., Mo H. J., Wang K., 2023, Massive Dark Matter Halos at High Redshift: Implications for Observations in the JWST Era ([arXiv:2304.13890](https://arxiv.org/abs/2304.13890))
- Chevallard J., Charlot S., 2016, *Monthly Notices of the Royal Astronomical Society*, 462, 1415
- Chiaki G., Chon S., Omukai K., Trinca A., Schneider R., Valiante R., 2023, *arXiv e-prints*, p. [arXiv:2303.01762](https://arxiv.org/abs/2303.01762)
- Curtis-Lake E., et al., 2022, Spectroscopy of four metal-poor galaxies beyond redshift ten, [doi:10.48550/ARXIV.2212.04568](https://arxiv.org/abs/2212.04568), <https://arxiv.org/abs/2212.04568>
- Davé R., Anglés-Alcázar D., Narayanan D., Li Q., Rafieeferantsoa M. H., Appleby S., 2019, *Monthly Notices of the Royal Astronomical Society*, 486, 2827
- Dekel A., Sarkar K. C., Birnboim Y., Mandelker N., Li Z., 2023, *MNRAS*, **523**, 3201
- Donnan C. T., et al., 2022, *Monthly Notices of the Royal Astronomical Society*, 518, 6011
- Finkelstein S. L., et al., 2022a, *arXiv e-prints*, p. [arXiv:2211.05792](https://arxiv.org/abs/2211.05792)
- Finkelstein S. L., et al., 2022b, *ApJ*, **940**, L55
- Harikane Y., et al., 2023, *ApJS*, **265**, 5
- Haslbauer M., Kroupa P., Zonoozi A. H., Haghi H., 2022, *The Astrophysical Journal Letters*, 939, L31
- Keller B. W., Munshi F., Trebitsch M., Tremmel M., 2023, *The Astrophysical Journal Letters*, 943, L28
- Kobayashi C., Ferrara A., 2023, *arXiv e-prints*, p. [arXiv:2308.15583](https://arxiv.org/abs/2308.15583)
- Komatsu E., et al., 2011, *ApJS*, **192**, 18
- Krumholz M. R., McKee C. F., 2005, *ApJ*, **630**, 250
- Kulkarni M., Visbal E., Bryan G. L., 2021, *ApJ*, **917**, 40
- Labbe I., et al., 2022, *arXiv e-prints*, p. [arXiv:2207.12446](https://arxiv.org/abs/2207.12446)
- Lovell C. C., Harrison I., Harikane Y., Tacchella S., Wilkins S. M., 2023, *MNRAS*, **518**, 2511
- Machacek M. E., Bryan G. L., Abel T., 2001, *ApJ*, **548**, 509
- Maiolino R., et al., 2023a, *arXiv e-prints*, p. [arXiv:2305.12492](https://arxiv.org/abs/2305.12492)
- Maiolino R., et al., 2023b, *arXiv e-prints*, p. [arXiv:2305.12492](https://arxiv.org/abs/2305.12492)
- Mason C. A., Trenti M., Treu T., 2023, *MNRAS*, **521**, 497
- McAlpine S., et al., 2016, *Astronomy and Computing*, **15**, 72
- Menci N., Castellano M., Santini P., Merlin E., Fontana A., Shankar F., 2022, *ApJ*, **938**, L5
- Murray S. G., Power C., Robotham A. S. G., 2013, *Astronomy and Computing*, **3**, 23
- Nagele C., Umeda H., 2023, *ApJ*, **949**, L16
- Naiman J. P., et al., 2018, *Monthly Notices of the Royal Astronomical Society*, 477, 1206
- Narayanan D., et al., 2023, Outshining by Recent Star Formation Prevents the Accurate Measurement of High- z Galaxy Stellar Masses ([arXiv:2306.10118](https://arxiv.org/abs/2306.10118))
- O’Shea B. W., Wise J. H., Xu H., Norman M. L., 2015, *ApJ*, **807**, L12
- Prada F., Behroozi P., Ishiyama T., Klypin A., Pérez E., 2023, *arXiv e-prints*, p. [arXiv:2304.11911](https://arxiv.org/abs/2304.11911)
- Robertson B. E., et al., 2022, Discovery and properties of the earliest galaxies with confirmed distances, [doi:10.48550/ARXIV.2212.04480](https://arxiv.org/abs/2212.04480), <https://arxiv.org/abs/2212.04480>
- Scholtz J., et al., 2023, *arXiv e-prints*, p. [arXiv:2306.09142](https://arxiv.org/abs/2306.09142)
- Sheth R. K., Tormen G., 1999, *MNRAS*, **308**, 119
- Smith B. D., Regan J. A., Downes T. P., Norman M. L., O’Shea B. W., Wise J. H., 2018, *MNRAS*, **480**, 3762
- Steinhardt C. L., Sneppen A., Clausen T., Katz H., Rey M. P., Stahlschmidt J., 2023, *arXiv e-prints*, p. [arXiv:2305.15459](https://arxiv.org/abs/2305.15459)
- Tacchella S., Bose S., Conroy C., Eisenstein D. J., Johnson B. D., 2018, *The Astrophysical Journal*, 868, 92
- Tan J. C., Krumholz M. R., McKee C. F., 2006, *ApJ*, **641**, L121
- Trebitsch M., et al., 2021, *A&A*, **653**, A154
- Tremmel M., et al., 2018, *Monthly Notices of the Royal Astronomical Society*, 483, 3336
- Ucci G., et al., 2021, cosmic_variance: Cosmic variance calculator, Astrophysics Source Code Library, record [ascl:2107.023](https://arxiv.org/abs/2107.023) ([ascl:2107.023](https://arxiv.org/abs/2107.023))
- Vogelsberger M., et al., 2014, *Nature*, 509, 177
- Wise J. H., Cen R., 2009, *ApJ*, **693**, 984
- Wise J. H., Turk M. J., Norman M. L., Abel T., 2012, *ApJ*, **745**, 50
- Wise J. H., Regan J. A., O’Shea B. W., Norman M. L., Downes T. P., Xu H., 2019, *Nature*, **566**, 85
- Xu H., Wise J. H., Norman M. L., 2013, *apj*, **773**, 83
- Xu H., Wise J. H., Norman M. L., Ahn K., O’Shea B. W., 2016, *The Astrophysical Journal*, 833, 84
- Yung L. Y. A., Somerville R. S., Finkelstein S. L., Wilkins S. M., Gardner J. P., 2023, Are the ultra-high-redshift galaxies at $z > 10$ surprising in the context of standard galaxy formation models? ([arXiv:2304.04348](https://arxiv.org/abs/2304.04348))

APPENDIX

APPENDIX A: CALCULATING THE NUMBER OF HALOES EXPECTED TO BE SEEN BY JWST

In Figure 2 we present predictions for the number of haloes of a certain stellar mass, M_* we expect to see in JWST's FoV, Ω , at a certain redshift, z . To do this we use the `hmf` module (Murray et al. 2013) to supply a halo mass function which we then use in our calculation. The halo mass function provides the number of haloes with a mass between M and $M + dm$ at z per comoving volume. The number of haloes we expect to see per comoving Mpc in JWST's field of view, with a mass greater than M_0 , is calculated as follows:

$$\frac{dn}{dr_c} = A(z) \int_{M_0}^{\infty} \frac{dn}{dm}(M, z) dm \quad (\text{A1})$$

$A(z)$, measured in Mpc^2 , is the comoving area at redshift z and is calculated from

$$A(z) = \Omega r_c^2(z) \quad (\text{A2})$$

where $r_c(z)$ is the comoving distance as a function of redshift. We can then convert it to the amount of haloes NIRCcam should observe per redshift with

$$\frac{dn}{dz} = \frac{dn}{dr_c} \frac{dr_c}{dz} \quad (\text{A3})$$

It is noted that effects due to dust extinction and the angular resolution of JWST's cameras are ignored for this calculation. For the field of view calculation, we use the FoV of the NIRCcam instrument (9.7 arcmin^2).